Periodic orbits and stability islands in chaotic seas created by separatrix crossings in slow-fast systems

Anatoly Neishtadt[1], Carles Simó[2], Dmitri Treschev[3], and Alexei Vasiliev[1]

[1] Space Research Institute, Profsoyuznaya 84/32, Moscow 117997, Russia,
[2] Departament de Matemàtica Aplicada i Anàlisi, Univ. de Barcelona, Gran Via, 585, Barcelona 08007, Spain,
[3] V. A. Steklov Mathematical Institute, Gubkina 8, Moscow 119991, Russia.

Abstract

We consider a 2 d.o.f. natural Hamiltonian system with one degree of freedom corresponding to fast motion and the other corresponding to slow motion. The Hamiltonian function is the sum of potential and kinetic energies, the kinetic energy being a weighted sum of squared momenta. The ratio of time derivatives of slow and fast variables is of order $\varepsilon \ll 1$. At frozen values of the slow variables there is a separatrix on the phase plane of the fast variables and there is a region in the phase space (the domain of separatrix crossings) where the projections of phase points onto the plane of the fast variables repeatedly cross the separatrix in the process of evolution of the slow variables. Under a certain symmetry condition we prove the existence of many, of order $1/\varepsilon$, stable periodic trajectories in the domain of the separatrix crossings. Each of these trajectories is surrounded by a stability island whose measure is estimated from below by a value of order ε. Thus, the total measure of the stability islands is estimated from below by a value independent of ε. We find the location of stable periodic trajectories and an asymptotic formula for the number of these trajectories. As an example, we consider the problem of motion of a charged particle in the parabolic model of magnetic field in the Earth magnetotail.

1 Introduction

Under general enough assumptions, in the phase space of a pendulum of a slow periodically varying length there exist many, of order $1/\varepsilon$, stable periodic trajectories. Along each of them, the pendulum transits from the oscillatory mode to the rotational one and back again [1, 2]. Here $\varepsilon > 0$ is a small parameter characterizing the rate of length variation. In the Poincaré section each of these periodic trajectories is represented by a stationary point surrounded by a stability island whose area is estimated from below by a value of order ε. Hence, the total area of the stability islands is estimated from below by a value independent of ε. Numerical experiments demonstrate that these islands are immersed into a chaotic sea and its measure can be estimated from below by a value independent of ε. However, rigorous estimates of this measure are not known.

The transition from one mode of the pendulum's motion to another corresponds to a crossing of the separatrix on the pendulum's phase portrait considered at a frozen value of its length. Similar results about stable periodic motions with separatrix crossings are valid in the problem of a particle's motion in a slowly periodically varying double-well potential [1, 2].

Analogous results can be obtained for 2 d.o.f. Hamiltonian systems with fast and slow variables (with one degree of freedom corresponding to the fast variables, and another one corresponding to the slow variables). At frozen values of the slow variables we obtain a 1 d.o.f. Hamiltonian system for the fast variables, called the fast system. This system involves values of the slow variables as parameters. Assume that on the phase portrait of the fast system there exists a saddle point, and the separatrices passing through this point form an "8"-like figure. As values of the slow variables change, the projections of the phase points onto the plane of the fast variables may cross the separatrix. Assume that the following symmetry condition is valid: the areas bounded by the two separatrix loops are equal at all possible values of the slow variables. Then, under certain additional conditions, on every energy level there are many, of order $1/\varepsilon$, stable periodic trajectories crossing the separatrix [3]. Here $\varepsilon > 0$ is a small parameter characterizing the ratio of time derivatives of slow and fast variables. Each one of these periodic trajectories is surrounded by stability island whose measure is estimated from below by a value of order ε. Hence, the total area of the stability islands is estimated from below by a value independent of ε [3].

The proofs in [1, 2] and [3] are based on the study of asymptotic formulas for the corresponding Poincaré maps. In [1, 2], these formulas were constructed with the use of asymptotic expressions for the jump of the adiabatic invariant at a separatrix crossing in systems with one and a half d.o.f. [4, 5, 6] and for the variation of the "angle" variable between separatrix crossings in such systems [7]. In [3], analogous formulas for systems with two d.o.f. [8, 9] were used.

In the present paper we consider a natural Hamiltonian system with two degrees of freedom corresponding to fast and slow motions; the Hamiltonian function is a sum of potential and kinetic energies, the kinetic energy is a weighted sum of squared momenta. This system possesses an additional symmetry allowing to locate the periodic trajectories and to find explicitly an asymptotic formula for their number. As main example we consider a model problem [10] of the motion of charged particles in the Earth magnetotail. The results can be also applied to some systems that are not natural but still possess the necessary additional symmetry. In particular, the results are applicable to the model system introduced in [11] to describe the motion of an asteroid near a 3:1 resonance with the Jupiter. The stability islands in this problem were found numerically in [12].

2 Main equations

Consider a 2 d.o.f. Hamiltonian system with the Hamiltonian function

$$H = \frac{1}{2}g(x)y^2 + \frac{1}{2}\beta(x)p^2 + U(q,x). \tag{1}$$

Here (p, q) and $(y, \varepsilon^{-1}x)$ are the pairs of canonically conjugated variables, $\varepsilon > 0$ is a small parameter. All the functions are assumed to be smooth enough, and the functions g and β are positive. The equations of motion have the form:

$$\dot{p} = -\frac{\partial H}{\partial q}, \quad \dot{q} = \frac{\partial H}{\partial p}, \quad \dot{y} = -\varepsilon\frac{\partial H}{\partial x}, \quad \dot{x} = \varepsilon\frac{\partial H}{\partial y}. \tag{2}$$

The variables p, q are called fast, while the variables y, x are called slow.

The system with Hamiltonian H at frozen values of the slow variables is called the fast system. It contains the value of x as a parameter. This is a natural system with one degree of freedom. Assume that the potential U is a symmetric function of q with two minima for all the considered values of x. The potential U has the local maximum at the point $q = q_s(x)$.

The phase portrait of the fast system is shown in Figure 1. On this phase portrait, there exist a non-degenerate saddle point C and separatrices l_1, l_2 passing through this point. These separatrices divide the (p, q)-plane into domains $G_i = G_i(x)$, $i = 1, 2, 3$. Introduce the function

$$E = \frac{1}{2}\beta(x)p^2 + U(q, x) - U(q_s(x), x). \tag{3}$$

In the domain G_3 the function E is positive, and in $G_{1,2}(x)$ it is negative. At the point C and on the separatrices $E = 0$.

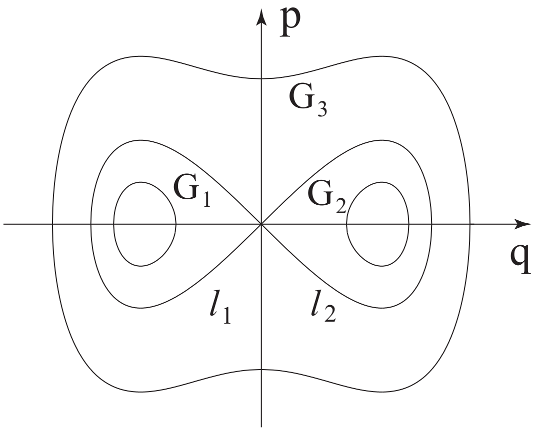

Figure 1: Phase portrait of the fast system.

Let $S = S(x)$ denote the area of $G_1(x)$. In the unperturbed system, one can introduce canonical "action-angle" variables (I, φ) separately in each G_i. The "action" I is a function of p, q, x given by the formula $I = I(E, x)$, where $I(e, x)$ is the area bounded by a trajectory of the fast system, corresponding to $E = e$, divided by 2π. The action is discontinuous on the separatrix, and hence it is convenient to introduce a modified action $\hat{I} = \hat{I}(E, x)$ coinciding with I at the points of $G_{1,2}$ and equal to $I/2$ at the points of G_3. On the separatrices and at the point C put $\hat{I} = S(x)/(2\pi)$. The function $\hat{I}$ is continuous.

For an approximate description of the motion in system (2) one can use the adiabatic approximation (see, e.g. [13]). In this approximation $\hat{I} = \text{const}$ along a phase trajectory, and the variation of the slow variables y, x is defined by a Hamiltonian system with Hamiltonian $H_0(I, y, x)$, where H_0 is the function H expressed in terms of I, y, x. Thus,

$H_0 = \frac{1}{2}g(x)y^2 + V(I,x)$, where $V(I,x)$ is the effective potential given by the function $\frac{1}{2}\beta(x)p^2 + U(q,x)$ expressed in terms of I, x. The system with the Hamiltonian H_0 is called the slow system. Let $\hat{H}_0 = \hat{H}_0(\hat{I}, y, x)$ denote the Hamiltonian H_0 expressed in terms of $\hat{I}, y, x$.

We shall consider trajectories of the slow system on an energy level $H_0 = h_0$. Along a trajectory $\hat{I} = \hat{I}(h_0 - \frac{1}{2}g(x)y^2 - U(q_s(x), x), x) = \text{const}$. Assume that on the plane of the slow variables there exists a domain (an annulus) $\mathcal{D}$ filled up by closed trajectories of the slow system with $H_0 = h_0$. The values of $\hat{I}$ corresponding to these trajectories fill up a segment Ξ.

Consider on the plane of variables (y, x) the uncertainty curve [11] $\Gamma = \Gamma(h_0) = \{y, x : \frac{1}{2}g(x)y^2 + U(q_s(x), x) = h_0\}$. We assume that every trajectory of the slow system that belongs to $\mathcal{D}$ crosses the uncertainty curve at exactly two points. Assume also that at these points $\Theta(y,x) \equiv gy\,\partial S/\partial x \neq 0$. Note that the points of intersection of a trajectory of the slow system with the uncertainty curve are symmetric with respect to the axis Oy. The uncertainty curve divides $\mathcal{D}$ into two subdomains $\mathcal{D}_3$ and $\mathcal{D}_{1,2}$. Consider a point $(y, x) \in \mathcal{D}_3$. The corresponding energy level line $H = h_0$ on the plane of the fast variables (p, q) belongs to the domain $G_3(x)$ and gives a trajectory of the fast system. For a point $(y, x) \in \mathcal{D}_{1,2}$ the corresponding energy level consists of two trajectories of the fast system, belonging to the domains G_1 and G_2 respectively. For a point $(y, x) \in \Gamma$ the energy level is the union of the separatrices $l_1(x), l_2(x)$ and the point $C(x)$.

3 Formulation of results

We look for stable periodic trajectories of system (2), belonging to the following three (discrete) families.

F1. The projection of the phase trajectory onto the plane of the slow variables is a closed curve. Along this curve the value of $\hat{I}$ oscillates with an amplitude $\mathrm{O}(\varepsilon)$ around a quantity $\hat{I}_0 \in \Xi$. The period of the motion along this trajectory differs by $\mathrm{O}(1)$ from the period of the motion along the trajectory $\hat{I} = \hat{I}_0 = \text{const}$ of the slow system. When the projection of the phase point onto the plane of the slow variables is in the domain $\mathcal{D}_{1,2}$ at a distance larger than $c_0\varepsilon$ from the uncertainty curve, the projection of the phase point onto the plane of the fast variables lies in G_1. Here c_0 is a large enough positive constant.

F2. The same as **F1** with G_1 replaced by G_2.

F(1,2). The same as **F1**, but the period of motion is $\mathrm{O}(1)$-close to the double of the period of motion along the corresponding trajectory of the slow system, and when the projection of the phase point onto the plane of the slow variables is in the domain $\mathcal{D}_{1,2}$ at a distance larger than $c_0\varepsilon$ from the uncertainty curve, the projection of the phase point onto the plane of the fast variables is in turn in the domains G_1 and G_2.

Theorem 1. Under additional generality conditions, on the energy level $H = h_0$ there are $\frac{K}{\varepsilon}(1 + \mathrm{o}(1))$ linearly stable periodic trajectories of each of the families **F1**, **F2**, and **F(1,2)**. Among the trajectories of both **F1** and **F2** there are $\frac{1}{\varepsilon}K_{sm}(1+\mathrm{o}(1))$ trajectories passing through points where $y = 0, p = 0$ (hence, they are symmetric). Among the trajectories of **F(1,2)** there are $\frac{1}{\varepsilon}K_{sm}(1+\mathrm{o}(1))$ trajectories passing through points where $y = 0, q = q_s(x) + o(1)$ (hence, they are nearly symmetric; if $q_s \equiv \text{const}$, these trajectories pass through the points with $y = 0, q = q_s$ and are symmetric). Here K, K_{sm} are positive constants; formulas for them are given in Section 7.

This theorem differs from the corresponding result of [3] in the following aspects: here we provide the explicit asymptotic formula for the number of the periodic trajectories, we include trajectories of **F(1,2)** into our consideration, and we describe the locations of the periodic trajectories (defined by the location of a point on the fast plane at $y=0$).

The phase space of system (2) is four-dimensional, and the energy level $H = h_0$ is three-dimensional. Therefore, if there is a two-dimensional invariant torus of the system, it divides the energy level into two invariant domains.

Prefix an arbitrary positive constant c_{00}.

Theorem 2. Under additional generality conditions, among the trajectories of each family, specified in Theorem 1, there are not less than $\frac{K-c_{00}^{-1}}{\varepsilon}$ (and, for symmetric and nearly symmetric trajectories, not less than $\frac{K_{sm}-c_{00}^{-1}}{\varepsilon}$) stable trajectories. Each of these trajectories is surrounded by an invariant torus, which bounds a domain of (3-dimensional) phase volume larger than $C_1^{-1}\varepsilon$. The variation of $\hat{I}$ in this domain is smaller than $C_2\varepsilon$.

Corollary. The total measure of these domains is larger than C_3^{-1}.

Here C_i are positive constants, i.e. values independent of ε.

This theorem differs from the corresponding result of [3] by the explicit estimate of the number of the stable trajectories. The necessary generality conditions are given in Sections 7 and 8.

Invariant tori in Theorem 2 are provided by the Kolmogorov-Arnold-Moser theory (KAM). In the domain bounded by each of these tori, there is a Cantor set of other invariant tori contractible to the periodic trajectory. Such domains are called stability islands.

4 Adiabatic and improved adiabatic approximations

In the fast system, the action-angle variables I, $\varphi \bmod 2\pi$ are introduced separately in each G_i by a canonical transformation of variables. The corresponding generating function $W(I,q,x)$ contains x as a parameter [for brevity, we omit the i subscripts]. We take this function in the form

$$W(I,q,x) = \int_{q_0(I,x)}^{q} \mathcal{P}(I,q',x)\mathrm{d}q', \tag{4}$$

where $\mathcal{P}$ is the value of the p-variable along the trajectory with the prescribed value of the action I. In G_1, G_2, $q_0(I,x)$ is the value of q at one of the two points where this trajectory crosses the axis $p=0$; in G_1 we take the right one of these points, and in G_2 we take the left one. In G_3 we take $q_0(I,x) = q_s(x)$ and assume that at this point $\mathcal{P} > 0$. In the new variables the Hamiltonian has the form $H = H_0(I,y,x)$.

Now make a canonical transformation of variables $(p,q,y,x) \mapsto (\bar{I},\bar{\varphi},\bar{y},\bar{x})$ with generating function $\bar{y}\varepsilon^{-1}x + W(\bar{I},q,x)$. The canonically conjugated pairs of variables are $(\bar{I},\bar{\varphi})$ and $(\bar{y},\varepsilon^{-1}\bar{x})$. The formulas for the transformation of variables are:

$$\bar{\varphi} = \partial W/\partial \bar{I}, \quad p = \partial W/\partial q, \quad \bar{x} = x, \quad y = \bar{y} + \varepsilon \partial W/\partial x. \tag{5}$$

In the new variables, the Hamiltonian H has the form

$$H = H_0(\bar{I},\bar{y},\bar{x}) + \varepsilon H_1(\bar{I},\bar{\varphi},\bar{y},\bar{x}) + \mathrm{O}(\varepsilon^2), \tag{6}$$

where

$$H_1 = g\bar{y}\frac{\partial W}{\partial x}. \tag{7}$$

In the adiabatic approximation, the dynamics is described by the Hamiltonian H_0. In this approximation $\bar{I} = \text{const}$ along a phase trajectory.

One can also construct a canonical, close to the identity, transformation of variables $(\bar{I}, \bar{\varphi}, \bar{y}, \bar{x}) \mapsto (J, \psi, \hat{y}, \hat{x})$ in order to make the terms of order ε in the Hamiltonian independent of the phase (see, for example, [13]). In the new variables, the Hamiltonian takes the form:

$$\mathcal{H} = H_0(J, \hat{y}, \hat{x}) + \varepsilon^2 \mathcal{H}_2(J, \psi, \hat{y}, \hat{x}, \varepsilon). \tag{8}$$

The term of order ε is absent because it is equal to the average of H_1 with respect to $\bar{\varphi}$, and this average is zero due to the symmetry with respect to the axis $p = 0$.

In the improved adiabatic approximation, the dynamics is described by the Hamiltonian $H_0(J, Y, X)$. In this approximation J is an integral of motion. With an accuracy of order ε^2, the following formula for J is valid (see [8]):

$$J = J(p, q, y, x) = I + \varepsilon u(p, q, y, x), \tag{9}$$

$$u = \frac{1}{2\pi} g y \int_0^T \left(\frac{T}{2} - t\right) \mathrm{d}t. \tag{10}$$

The integral here is calculated along a phase trajectory of the fast system passing through the point (p, q); t is the time of motion along this trajectory starting from this point, T is the period of the motion. The function J is the improved adiabatic invariant. In the complete system far from separatrices its value along a phase trajectory is constant with an accuracy of order ε^2 on time intervals of order ε^{-1}. In what follows, it is convenient to use the function $\hat{J}(p, q, y, x)$ equal to J in domains G_1, G_2 and equal to $J/2$ in domain G_3.

5 Description of separatrix crossing

On the phase plane $\mathbb{P}^{sl}$ of the slow variables (y, x), the separatrix is represented by a uncertainty curve $\Gamma(h_0)$ (see figure 2). The annulus $\mathcal{D}$ filled up with trajectories of the slow system with $\hat{I} \in \Xi$ is divided by the uncertainty curve into two domains $\mathcal{D}_3$ and $\mathcal{D}_{1,2}$. The ring $\mathcal{D}$ intersects the axis $y = 0$ along two segments $\mathcal{S}_3$ and $\mathcal{S}_{1,2}$, which belong to $\mathcal{D}_3$ and $\mathcal{D}_{1,2}$ respectively. The points on the fast plane corresponding to $\mathcal{S}_3$ belong to G_3, and the points corresponding to $\mathcal{S}_{1,2}$ belong to G_1 and G_2. Fix an interval $\Xi_0 \in \Xi$, such that the endpoints of Ξ_0 and Ξ are different.

Let the motion start at time $t = 0$ in a point $M^{(0)}(p^{(0)}, q^{(0)}, y^{(0)}, x^{(0)})$, such that $(\hat{y}^{(0)}, \hat{x}^{(0)}) \in \mathcal{S}_3$. Hence, $(p^{(0)}, q^{(0)}) \in G_3(x^{(0)})$. Let $\hat{I} = \hat{I}^{(0)}$, $\hat{J} = \hat{J}^{(0)}$, $\psi = \psi^{(0)}$ at this point; $\hat{I}^{(0)} \in \Xi_0$. In the adiabatic approximation the trajectory of the slow variables is $B(\hat{I}^{(0)}) = \{y, x \,:\, \hat{H}_0(\hat{I}^{(0)}, y, x) = h_0\}$, the motion is described by a Hamiltonian system with Hamiltonian $H_0(\hat{I}^{(0)}, y, x)$. Let (x_*, y_*) and $(x_*, -y_*)$ denote points of intersection of $B(\hat{I}^{(0)})$ and $\Gamma(h_0)$. Assume, for definiteness, that $y_* > 0$, $\Theta_* \equiv \Theta(y_*, x_*) > 0$. Thus, a phase point of the slow system passes from $\mathcal{D}_3$ to $\mathcal{D}_{1,2}$ at the point (x_*, y_*), and at the

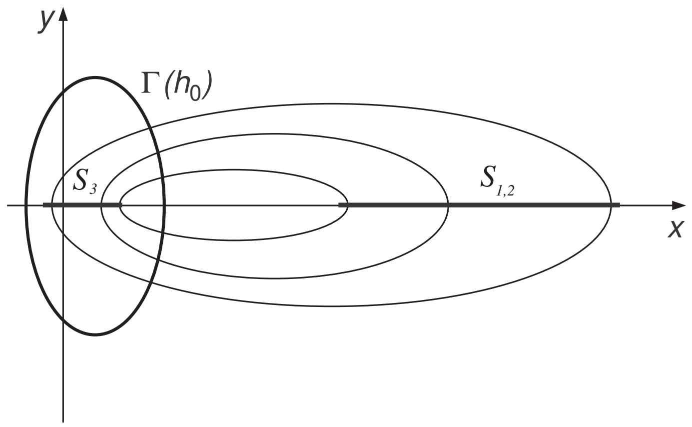

Figure 2: Schematic picture of the motion on the slow plane.

point $(x_*, -y_*)$ it passes from $\mathcal{D}_{1,2}$ to $\mathcal{D}_3$. Below τ_* and τ_{**} denote the slow time moments of separatrix crossing in this approximation. (Slow time is $\tau = \varepsilon t$.) In the exact system, in the process of evolution the phase point on the plane of the slow variables approaches the curve $\Gamma(h_0)$, and accordingly, on the plane (p, q) it approaches the separatrix. We are interested in the dynamics of phase points that are being captured into G_ν, $\nu = 1, 2$ after the separatrix crossing. For such a phase point, the first crossing of Cq-axis in G_ν (see Figure 1) occurs near C at time $\tau = \tau_* + \mathrm{O}(\varepsilon)$. Assuming that at the point of this crossing $E = h^{(0)}$, we introduce $\eta^{(0)} = 1 - |h^{(0)}/\varepsilon\Theta_*|$.

After the separatrix crossing the phase point in the plane of the slow variables $(\hat{y}, \hat{x})$ moves towards $\mathcal{S}_{1,2}$. When it crosses $\mathcal{S}_{1,2}$, the projection of the phase point onto the fast plane is deep inside the region G_ν. Denote the value of $\hat{J}$ at this time moment as $\hat{J}^{(1)}$.

Then the phase point starts again approaching the separatrix. At $\tau = \tau_{**} + \mathrm{O}(\varepsilon)$ the phase point crosses Cq-axis in G_ν near the point C for the last time before entering G_3. Assuming that at the point of this crossing $E = h^{(1)}$, we introduce $\eta^{(1)} = |h^{(1)}/\varepsilon\Theta_*|$.

After crossing $\Gamma(h_0)$, the projection of the phase point onto the plane $(\hat{y}, \hat{x})$ crosses again the segment $\mathcal{S}_3$. Let $\hat{J}^{(2)}$, $\psi^{(2)}$ denote the values of $\hat{J}$, ψ at this time moment. Then the phase point approaches the separatrix again, crosses it and gets captured into the domain G_l, $l = 1$ or $l = 2$. Let E be equal to $h^{(2)}$ at the first crossing of the Cq-axis in G_l near C. This crossing occurs at time $\tau = \tau_* + T_0 + \mathrm{O}(\varepsilon)$, where T_0 is the slow time period of motion along the trajectory $\hat{I} = \hat{I}^{(0)}$ in the adiabatic approximation. We introduce $\eta^{(2)} = 1 - |h^{(2)}/\varepsilon\Theta_*|$.

6 The return map

In the energy level $H = h_0$ the segment $\mathcal{S}_3$ is represented by a piece of a two-dimensional surface $\{p, q, y, x : H(p, q, y, x) = h_0, (\hat{y}, \hat{x}) \in \mathcal{S}_3\}$. This piece can be parametrized by variables $\hat{J}, \psi$. The corresponding Poincaré return map $M : (\hat{J}^{(0)}, \psi^{(0)}) \to (\hat{J}^{(2)}, \psi^{(2)})$ produced by trajectories that pass through G_ν is symplectic. Its stable stationary points correspond to stable periodic orbits of the original problem, of period approximately equal to T_0/ε. It is convenient to study these stationary points using a different set of variables, namely to consider the map $\hat{M} : (\hat{J}^{(0)}, \eta^{(0)}, \nu) \to (\hat{J}^{(2)}, \eta^{(2)}, l)$.

The map $\hat{M}$ is the composition of two maps: $\hat{M} = M^{(2)} \circ M^{(1)}$,

$$M^{(1)} : (\hat{J}^{(0)}, \eta^{(0)}, \nu) \to (\hat{J}^{(1)}, \eta^{(1)}, \nu)\,, \quad M^{(2)} : (\hat{J}^{(1)}, \eta^{(1)}, \nu) \to (\hat{J}^{(2)}, \eta^{(2)}, l)\,.$$

The results of [8, 9] give the following formulas for $M^{(k)}$. Prefix an arbitrary positive constant c_1. Suppose that

$$\eta^{(0)}, \eta^{(1)}, \eta^{(2)} \in [c_1^{-1}, 1 - c_1^{-1}]\,. \tag{11}$$

Then

$$\begin{aligned} \hat{J}^{(1)} &= \hat{J}^{(0)} - (2\pi)^{-1}\varepsilon a_* \Theta_* \ln(2\sin\pi\eta^{(0)}) + O(\varepsilon^{3/2}\ln\varepsilon)\,, && (12)\\ \eta^{(1)} &= \{\eta^{(0)} + \varepsilon^{-1}\Phi_1(\hat{J}^{(1)}) + O(\varepsilon^{1/3}\ln^{-1/3}\varepsilon)\}\,, && (13) \end{aligned}$$

$$\begin{aligned} \hat{J}^{(2)} &= \hat{J}^{(1)} + (2\pi)^{-1}\varepsilon a_* \Theta_* \ln(2\sin\pi\eta^{(1)}) + O(\varepsilon^{3/2}\ln\varepsilon)\,, && (14)\\ \eta^{(2)} &= \{\eta^{(1)} + \varepsilon^{-1}\Phi_2(\hat{J}^{(2)}) + O(\varepsilon^{1/3}\ln^{-1/3}\varepsilon)\}\,, && (15) \end{aligned}$$

$$\begin{aligned} &l = \nu, && \text{if} \quad 0 < \{(\varepsilon^{-1}\Phi_2(\hat{J}^{(2)}) + \eta^{(1)})/2\} < 1/2, && (16)\\ &l \neq \nu, && \text{if} \quad 1/2 < \{(\varepsilon^{-1}\Phi_2(\hat{J}^{(2)}) + \eta^{(1)})/2\} < 1. && (17) \end{aligned}$$

Here $\{\,\cdot\,\}$ denotes the fractional part, $a_* = a(x_*)$. The value of a is given by $a = 1/\sqrt{-d}$, where d is the Hessian of E at the point C. In (13), (15) one has introduced

$$\begin{aligned} \Phi_1(\hat{J}) &= \frac{1}{2\pi}\int_{\tau_-^{(1)}}^{\tau_+^{(1)}} (\omega_0^{(1)}(\hat{J}, Y_1(\tau), X_1(\tau)))\,\mathrm{d}\tau\,, && (18)\\ \Phi_2(\hat{J}) &= \frac{1}{\pi}\int_{\tau_+^{(3)}}^{\tau_-^{(3)}} (\omega_0^{(3)}(2\hat{J}, Y_3(\tau), X_3(\tau)))\,\mathrm{d}\tau. && (19) \end{aligned}$$

Here $\omega_0^{(j)} = \partial H_0/\partial J$, with H_0 calculated in the region G_j, and (Y_j, X_j) is a solution of a Hamiltonian system with Hamiltonian $H_0(J, y, x)$ on the energy level $H_0 = h_0$. The values $\tau_\pm^{(j)}$ are the slow time moments when the phase point corresponding to this solution arrives to the separatrix. At these moments $S(Y, X) = 2\pi\hat{J}$. [One can take any of such solutions, they differ by a time shift which does not change the value of the integrals in (18), (19)]. The conditions (11) are understood inductively: if $\eta^{(0)} \in [c_1^{-1}, 1 - c_1^{-1}]$, and $\eta^{(1)}$, found according to (12), (13) lies in the segment $[c_1^{-1}, 1 - c_1^{-1}]$, then (13) is valid, and analogously for $\eta^{(2)}$ and expressions (14), (15).

Equations (12), (14) follow directly from the formula for the jump of the adiabatic invariant at a separatrix [8] in case the assumed symmetry properties hold. Equation (13) follows directly from the formula for the phase change between separatrix crossings [9]. Equations (15)-(17) follow from the result of [9] in the following way.

Let h_+ be the value of E when the phase point crosses the axis Cp near C for the first time after exit from G_ν. At this time moment the phase point is in G_3 on the positive or the negative part of the axis Cp. Let h_- be the value of E when the phase point crosses the same part of Cp for the last time before exit from G_3. Introduce the notations: $\bar\zeta = \frac{h_+}{2\varepsilon|\Theta_*|}$, $\zeta = \frac{h_-}{2\varepsilon|\Theta_*|}$. According to [9],

$$\bar\zeta + \zeta = \frac{1}{2\varepsilon}\Phi_2(\hat J^{(1)}) + O(\varepsilon^{1/3}\ln^{-1/3}\varepsilon) \bmod 1, \tag{20}$$

provided $\bar\zeta, \zeta \in [c_2^{-1}, 1 - c_2^{-1}]$. The values $h^{(1)}$ (see Section 5) and h_+ are related as $h_+ = h^{(1)} + \varepsilon\Theta_* + \mathrm{O}(\varepsilon^{3/2})$ [8]. Therefore, $\bar\zeta = \frac{1}{2}(1-\eta^{(1)}) + \mathrm{O}(\varepsilon^{1/2})$. The values $h^{(2)}$ (see Section 5) and h_- are related as $h_- = h^{(2)} + 2\varepsilon\Theta_* + \mathrm{O}(\varepsilon^{3/2})$ if $l = \nu$, and as $h_- = h^{(2)} + \varepsilon\Theta_* + \mathrm{O}(\varepsilon^{3/2})$ if $l \neq \nu$. We have $l = \nu$ provided that $1/2 < \zeta < 1$. Consider this case. We obtain that $\zeta = \frac{1}{2}(1+\eta^{(2)}) + \mathrm{O}(\varepsilon^{1/2})$. From (20) we find

$$\frac{1}{2}(1-\eta^{(1)}) + \frac{1}{2}(1+\eta^{(2)}) = \frac{1}{2\varepsilon}\Phi_2(\hat J^{(2)}) + O(\varepsilon^{1/3}\ln^{-1/3}\varepsilon) \bmod 1.$$

Therefore,

$$\eta^{(2)} = \eta^{(1)} + \frac{1}{\varepsilon}\Phi_2(\hat J^{(2)}) + O(\varepsilon^{1/3}\ln^{-1/3}\varepsilon) \bmod 2. \tag{21}$$

Then condition $1/2 < \zeta < 1$ implies equation (16).

Now consider the case $l \neq \nu$. In this case $0 < \zeta < 1/2$. We get that ζ and $\eta^{(2)}$ are related as $\zeta = \frac{1}{2}\eta^{(2)} + \mathrm{O}(\varepsilon^{1/2})$. From (20) we find

$$\frac{1}{2}(1-\eta^{(1)}) + \frac{1}{2}\eta^{(2)} = \frac{1}{2\varepsilon}\Phi_2(\hat J^{(2)}) + O(\varepsilon^{1/3}\ln^{-1/3}\varepsilon) \bmod 1.$$

Therefore,

$$\eta^{(2)} = \eta^{(1)} + \frac{1}{\varepsilon}\Phi_2(\hat J^{(2)}) - 1 + O(\varepsilon^{1/3}\ln^{-1/3}\varepsilon) \bmod 2. \tag{22}$$

Combining (21) and (22) we obtain equation (15). Condition $0 < \zeta < 1/2$ implies (17).

7 Linearly stable periodic trajectories

7.1 Equations for stable fixed points

Linearly stable periodic trajectories of the original problem belonging to the families **F1**, **F2** correspond to linearly stable fixed points of the map $\hat M$. These points are defined by the following set of conditions:

$$\hat J^{(2)} = \hat J^{(0)}, \quad \eta^{(2)} = \eta^{(0)}, \quad l = \nu, \tag{23}$$

$$|\,\mathrm{tr}\,\hat M'\,| < 2, \tag{24}$$

where $\hat M'$ is the linearization of $\hat M$ at the fixed point, ν equals 1 or 2. To find solutions of the family $\mathbf{F(1,2)}$ one should replace the last relation in (23) with $l \neq \nu$.

Consider for definiteness solutions of the family **F1**. Introduce the following notations:

$$\hat J^{(s)} = \varepsilon\xi^{(s)}, \quad s = 0, 1, 2; \tag{25}$$

$$\varepsilon^{-1}\frac{d\Phi_k(\varepsilon\xi)}{d\xi} = \gamma_k(\varepsilon\xi), \qquad a_*\Theta_* = 2\pi\alpha.$$

Suppose that $(\xi^{(0)}, \eta^{(0)}) = (\xi, \eta)$ correspond to a fixed point of the map $\hat{M}$. We rewrite equations (23) using formulas (11)-(15), notations (25), and neglecting terms $O(\varepsilon^{1/3}\ln^{-1/3}\varepsilon)$:

$$\sin \pi\eta = \sin \pi\eta^{(1)}, \tag{26}$$

$$\eta^{(1)} - \eta + \gamma_1\alpha \ln(2\sin \pi\eta) = \varepsilon^{-1}\Phi_1(\varepsilon\xi) \bmod 1, \tag{27}$$

$$\eta - \eta^{(1)} = \varepsilon^{-1}\Phi_2(\varepsilon\xi) \bmod 2, \tag{28}$$

$$\eta, \eta^{(1)} \in (c_1^{-1}, 1 - c_1^{-1}). \tag{29}$$

Note that equation (28) implies $l = \nu$ (cf. (21)).

The stability condition $|\operatorname{tr} \hat{M}'| < 2$ can be written using (12)-(15) [we again neglect terms $O(\varepsilon^{1/3}\ln^{-1/3}\varepsilon)$]:

$$-4 < Q < 0, \tag{30}$$

$$Q = (u_2 - u_1)(\gamma_2 + \gamma_1) - u_2 u_1 \gamma_2 \gamma_1, \tag{31}$$

$$u_1 = \alpha\pi \cot \pi\eta, \quad u_2 = \alpha\pi \cot \pi\eta^{(1)}.$$

The exact set of conditions for a stable periodic solution differs from (26)-(29) by terms $O(\varepsilon^{1/3}\ln^{-1/3}\varepsilon)$ that can be differentiated in $\varepsilon\xi\,, \eta\,, \eta^{(1)}$ without changing their smallness order. Below, we find non-degenerate solutions of system (26)-(29). According to the implicit function theorem, for small enough ε, each of these solutions corresponds to a solution of the exact system.

7.2 Existence of stable fixed points

We assume that the following generality conditions are valid.

H1. For almost all $I \in \Xi_0$

$$\gamma_1(I) \cdot \gamma_2(I) \neq 0\,, \qquad \frac{\mathrm{d}}{\mathrm{d}I}(\gamma_1(I)/\gamma_2(I)) \neq 0\,. \tag{32}$$

Equation (26) implies that either $\eta^{(1)} = \eta$ or $\eta^{(1)} = 1 - \eta$. First, consider the case $\eta^{(1)} = \eta$. The system (27), (28) takes the form:

$$\gamma_1\alpha\ln(2\sin \pi\eta) = \varepsilon^{-1}\Phi_1(\varepsilon\xi) \bmod 1, \tag{33}$$

$$0 = \varepsilon^{-1}\Phi_2(\varepsilon\xi) \bmod 2. \tag{34}$$

From (31) we have:

$$-4 < -u^2\gamma_2\gamma_1 < 0,\ u = \alpha\pi \cot \pi\eta. \tag{35}$$

If $\gamma_2\gamma_1 < 0$, the inequality (35) cannot be satisfied.

If $\gamma_2\gamma_1 > 0$, the inequality (35) gives

$$|\eta - 1/2| < \frac{1}{\pi} \arctan \frac{2}{\alpha\pi\sqrt{\gamma_1\gamma_2}}. \tag{36}$$

This condition implies (29), provided the constant c_1 is large enough.

Now consider the second case, $\eta^{(1)} = 1 - \eta$. The system (27), (28) takes the form:

$$-2\eta + \gamma_1 \alpha \ln(2\sin\pi\eta) = \varepsilon^{-1}\Phi_1(\varepsilon\xi) \bmod 1, \tag{37}$$
$$2\eta - 1 = \varepsilon^{-1}\Phi_2(\varepsilon\xi) \bmod 2. \tag{38}$$

From (31) we have:

$$-4 < -2u(\gamma_2 + \gamma_1) + u^2\gamma_2\gamma_1 < 0,\; u = \alpha\pi\cot\pi\eta. \tag{39}$$

This inequality has solutions for any γ_1, γ_2. Consider, for example, the case $\gamma_1 < 0, \gamma_2 > 0, |\gamma_1| > \gamma_2$. In this case, (39) is satisfied at

$$-\frac{2}{|\gamma_1|} < u < 0 \quad \text{or} \quad 2\left(\frac{1}{\gamma_1} + \frac{1}{\gamma_2}\right) < u < \frac{2}{\gamma_2}, \tag{40}$$

and the corresponding intervals of η are:

$$0 < \eta - \frac{1}{2} < \frac{1}{\pi}\arctan\frac{2}{\alpha\pi|\gamma_1|}\,,$$
$$\frac{1}{\pi}\arctan\frac{2}{\alpha\pi\gamma_2} < \eta - \frac{1}{2} < -\frac{1}{\pi}\arctan\left(\frac{2}{\alpha\pi}\left(\frac{1}{\gamma_1} + \frac{1}{\gamma_2}\right)\right). \tag{41}$$

These inequalities also imply (29), provided the constant c_1 is large enough.

The system (26)-(28), equivalent to (33), (34) unified with (37), (38), can be interpreted geometrically as follows. R.h.s of equations (27), (28) defines a point $\varepsilon^{-1}\Phi(\varepsilon\xi) = (\varepsilon^{-1}\Phi_1(\varepsilon\xi) \bmod 1,\, \varepsilon^{-1}\Phi_2(\varepsilon\xi) \bmod 2)$ on the torus $\mathbb{T}^2 = \{(s_1 \bmod 1, s_2 \bmod 2)\}$. As ξ varies, this point is moving fast, with its velocity vector $\gamma(\varepsilon\xi) = (\gamma_1(\varepsilon\xi)\,, \gamma_2(\varepsilon\xi))$ varying slowly. L.h.s. of equations (27), (28), and (26), together with stability condition (30) define a set $\Lambda(\varepsilon\xi) \subset \mathbb{T}^2$ parametrized by η and an index distinguishing systems (33), (34) and (37), (38). It was shown above, that this set is the union of several (two or three) segments of curves. For brevity we call the set $\Lambda(\varepsilon\xi)$ a curve. As ξ varies, $\Lambda(\varepsilon\xi)$ slowly moves on the torus. Solutions of (26)-(28), (30) correspond to values of "time" ξ when the point $\varepsilon^{-1}\Phi(\varepsilon\xi)$ crosses, in its motion on the torus, the curve $\Lambda(\varepsilon\xi)$.

It follows from assumption **H1** that at almost all $I \in \Xi$ the winding on the torus with frequency vector $\gamma(I)$ is ergodic and transversal to $\Lambda(I)$ at almost all points of $\Lambda(I)$. Hence, it is possible to calculate, in the main approximation, the number of the points of intersection (cf. [14]). This number is $(K + o(1))/\varepsilon$, where

$$K = \frac{1}{2}\int_{\Xi_0}\Big(\int_{\Lambda(I)} |(\gamma(I),\, n(l, I))|\,\mathrm{d}l\Big)\,\mathrm{d}I. \tag{42}$$

Here l is the natural parameter on $\Lambda(I)$, and $n(l, I)$ is a unit normal vector on $\Lambda(I)$. The factor $1/2$ in this formula is due to the fact that the area of the surface of the torus equals 2. The value of the inner integral in (42) equals the product of the length of vector $\gamma(I)$ and the full length of the projection of the curve $\Lambda(I)$ onto the normal to vector $\gamma(I)$.

The curve $\Lambda(I)$ is the union of two curves $\Lambda_{nsm}(I)$ and $\Lambda_{sm}(I)$ constructed according to systems (33)-(35) and (37)-(39) respectively. Hence the value K can also be represented as $K = K_{nsm} + K_{sm}$, where K_{nsm} and K_{sm} are given by (42) with Λ replaced by Λ_{nsm} or Λ_{sm}. The subscripts "sm" and "nsm" are abbreviations for "symmetric" and "non-symmetric".

In the following section we show that indeed, system (37)-(39) gives symmetric or nearly symmetric periodic trajectories.

From the results obtained above we find that if $\gamma_2\gamma_1 < 0$, $K_{nsm} = 0$. If $\gamma_2\gamma_1 > 0$, Λ_{nsm} is a doubled segment of the s_1-axis on the torus: as η covers the interval (36), this segment is covered twice. Hence, to calculate the length of Λ_{nsm}, one should multiply by four the magnitude of the difference between the values of the function $\gamma_1\alpha\ln(2\sin\pi\eta)$ at the middle point and at the end point of the interval (36). Thus, this length equals

$$4|\gamma_1|\alpha\left(\ln 2 - \ln\left(2\cos\arctan\frac{2}{\alpha\pi\sqrt{\gamma_1\gamma_2}}\right)\right) = \\ 2|\gamma_1|\alpha\ln\left(1+\frac{4}{\alpha^2\pi^2\gamma_1\gamma_2}\right).$$

From formula (42) we obtain:

$$K_{nsm} = \int_{\Xi_0}\alpha\gamma_1\gamma_2\ln\left(1+\frac{4}{\alpha^2\pi^2\gamma_1\gamma_2}\right)\,\mathrm{d}I. \tag{43}$$

Now we shall obtain a formula for K_{sm} under the assumptions $\gamma_1 < 0, \gamma_2 > 0, |\gamma_1| > \gamma_2$; the results are analogous for the other cases. The projection of a point on the curve Λ_{sm} onto the normal to the vector γ multiplied by the length of γ is

$$f(\eta) = \gamma_2(-2\eta + \gamma_1\alpha\ln(2\sin\pi\eta)) - \gamma_1(2\eta-1). \tag{44}$$

The derivative of this function is zero only at the right end of the second of the intervals (41). Therefore, on both intervals (41) the function f is monotonous, increasing on the first interval and decreasing on the second one. Hence, the product $\chi(I)$ of the length of γ and the length of the projection of Λ_{sm} onto the normal to the vector γ equals the sum of the magnitudes of the differences between values of f at the endpoints of the intervals (41):

$$\chi(I) = -(\gamma_1+\gamma_2)\frac{2}{\pi}\arctan\frac{2}{\alpha\pi|\gamma_1|} - \frac{1}{2}\gamma_1\gamma_2\ln\left(1+\frac{4}{\alpha^2\pi^2\gamma_1^2}\right) + \\ (\gamma_1+\gamma_2)\frac{2}{\pi}\left(\arctan\frac{2}{\alpha\pi\gamma_2} - \arctan\left(\frac{2}{\alpha\pi}\left(\frac{1}{\gamma_1}+\frac{1}{\gamma_2}\right)\right)\right) + \\ \frac{1}{2}\gamma_1\gamma_2\alpha\left(\ln\left(1+\frac{4}{\alpha^2\pi^2}\left(\frac{1}{\gamma_1}+\frac{1}{\gamma_2}\right)^2\right) - \ln\left(1+\frac{4}{\alpha^2\pi^2\gamma_2^2}\right)\right).$$

For K_{sm} we have

$$K_{sm} = \frac{1}{2}\int_{\Xi_0}\chi(I)\,\mathrm{d}I. \tag{45}$$

The obtained formulas give the number of periodic trajectories of the family **F1** in the main approximation. The number of periodic trajectories of **F2** or **F(1,2)** is the same in the main approximation. For trajectories of **F2** the argument is the same. For trajectories of **F(1,2)** the equation (28) should be replaced by

$$\eta - \eta^{(1)} = \varepsilon^{-1}\Phi_2(\varepsilon\xi) + 1 \bmod 2 \tag{46}$$

and equations (34), (38) should be changed accordingly. The rest of the argument is as before.

If we omit the stability condition $|\operatorname{tr}\hat{M}'| < 2$ in the definition of the curves $\Lambda, \Lambda_{nsm}, \Lambda_{sm}$, the obtained formulas for K, K_{nsm}, K_{sm} give an asymptotic estimate of the total number of periodic trajectories and the number of periodic trajectories with $\eta^{(1)} = \eta$ or $\eta^{(1)} = 1-\eta$ satisfying the condition $\eta, \eta^{(1)}, \eta^{(2)} \in [c_1^{-1}, 1-c_1^{-1}]$. Hence the number of unstable periodic trajectories is also at least of order $\mathrm{O}(\varepsilon^{-1})$.

In the limit as $\varepsilon \to 0$ one can define in a natural way the distribution density of the number of periodic trajectories at a fixed value of I as a function of η. From formulas (42), (33), (34) we find that for trajectories with $\eta^{(1)} = \eta$ this density equals

$$\mathrm{const}(I)|\cot \pi\eta|.$$

From formulas (42), (37), (38) we find that for trajectories with $\eta^{(1)} = 1-\eta$ this density is

$$\mathrm{const}(I)\left|\frac{2(\gamma_1+\gamma_2)}{\alpha\pi\gamma_1\gamma_2} - \cot \pi\eta\right|. \tag{47}$$

7.3 Symmetry properties of the trajectories

Periodic trajectories of the families **F1** and **F2** that correspond to the set Λ_{sm} are symmetric. Indeed, for these trajectories $\eta^{(1)} = 1-\eta$ and, according to (38),

$$2\eta - 1 = \varepsilon^{-1}\Phi_2(\hat{J}^{(0)}) + \mathrm{O}(\varepsilon^{1/3}\ln^{-1/3}\varepsilon) \bmod 2.$$

For the value ζ introduced at the end of Section 6 we have

$$\zeta = \frac{1}{2}(1+\eta) + \mathrm{O}(\varepsilon^{1/2}), \tag{48}$$

therefore,

$$4\zeta - 1 = \varepsilon^{-1}\Phi_2(\hat{J}^{(0)}) + \mathrm{O}(\varepsilon^{1/3}\ln^{-1/3}\varepsilon) \bmod 2. \tag{49}$$

Let φ_0 denote the value of the "angle" variable φ at the initial point $M^{(0)}$ of the considered trajectory (for definiteness, let the trajectory be of the family **F1**). According to [9]

$$\zeta = \frac{1}{2\pi}\varphi_0 + \frac{1}{4\varepsilon}\Phi_2(\hat{J}^{(0)}) + \mathrm{O}(\varepsilon^{1/3}\ln^{-1/3}\varepsilon) \bmod 1. \tag{50}$$

Expressing ζ from (49) and substituting in (50) we find:

$$\frac{\varphi_0}{2\pi} = \frac{1}{4} + \mathrm{O}(\varepsilon^{1/3}\ln^{-1/3}\varepsilon) \bmod 1/2.$$

Hence, possible values of φ_0 are $\pi/2 + \mathrm{O}(\varepsilon^{1/3}\ln^{-1/3}\varepsilon)$ and $3\pi/2 + \mathrm{O}(\varepsilon^{1/3}\ln^{-1/3}\varepsilon)$. Therefore at $t=0$, when $y=0$, the phase point on the plane of the fast variables is located nearby the axis $p=0$. In fact, at $t=0$ we have $p=0$. Indeed, it follows from the symmetry of the problem that together with the periodic solution $(p(t), q(t), y(t), x(t))$ also exists the periodic solution $(-p(-t), q(-t), -y(-t), x(-t))$. At $t=0$, on these two solutions the values of y, x, J coincide, and the values of φ are close. If these two periodic solutions were different, system (37)-(39) would have two solutions with $\varepsilon\xi = \hat{J}^{(0)}$ and close values of η. This contradicts the non-degeneracy of system (37)-(39). Hence, initially $p=0$ and the considered periodic trajectory is symmetric:

$$(p(t), q(t), y(t), x(t)) \equiv (-p(-t), q(-t), -y(-t), x(-t)).$$

Periodic trajectories of the family **F(1,2)** that correspond to the set Λ_{sm} are nearly symmetric. Using (22) and $\eta + \eta^{(1)} = 1$, we obtain for such trajectories

$$2\eta = \varepsilon^{-1}\Phi_2(\hat{J}^{(0)}) + \mathrm{O}(\varepsilon^{1/3}\ln^{-1/3}\varepsilon) \bmod 2. \tag{51}$$

From (48) we find

$$4\zeta = \varepsilon^{-1}\Phi_2(\hat{J}^{(0)}) + \mathrm{O}(\varepsilon^{1/3}\ln^{-1/3}\varepsilon) \bmod 2. \tag{52}$$

Using (50) we obtain

$$\frac{\varphi_0}{2\pi} = \mathrm{O}(\varepsilon^{1/3}\ln^{-1/3}\varepsilon) \bmod 1/2.$$

Therefore, possible values of φ_0 are $\mathrm{O}(\varepsilon^{1/3}\ln^{-1/3}\varepsilon)$ and $\pi + \mathrm{O}(\varepsilon^{1/3}\ln^{-1/3}\varepsilon)$. Hence, at $t=0$, when $y=0$, the phase point on the plane of the fast variables has a value of q close to $q_s(x^{(0)})$. If $q_s \equiv$ const, the reflection w.r.t. the plane $q = q_s, y = 0, t = 0$ is a canonical transformation. In this case, it can be shown as above that at $t=0$ we have $q = q_s$, and the periodic trajectory is symmetric with respect to the plane $q = q_s$.

8 Stability islands

Let ξ_r, η_r, $\eta_r^{(1)}$ be one of the solutions of system (26)-(31), found in the previous section. One can rewrite the map $\hat{M}$ in the variables $\tilde{\xi} = \xi - \xi_r$, η, expand its right hand sides in ε supposing $\tilde{\xi} \sim 1$, and neglect terms $\mathrm{O}(\varepsilon^{1/3}\ln^{-1/3}\varepsilon)$. Thus, one obtains a map that does not contain ε and depends on the parameter $I_r = \varepsilon\xi_r$. This map has a stationary linearly stable point $\tilde{\xi} = 0$, $\eta = \eta_r$. According to Kolmogorov-Arnold-Moser (KAM) theory, under certain conditions [absence of resonances up to the 4-th order, non-zero coefficient in the normal form] the stationary point of the complete map is surrounded with a Cantor family of invariant curves (see, e.g. [13]). These latter conditions of KAM theory in the case under consideration can be written as one condition, namely $F(I_r, \eta_r) \neq 0$, where F is a piecewise smooth function. We assume that the following condition is valid.

H2. For all $I \in \Xi_0$ we have $F(I_*, \eta_*) \neq 0$ at all $\eta \in (0,1)$ except, maybe, at a finite number of points whose location depends on I piecewise smoothly.

Prefix an arbitrary constant $c_2 > 0$. Let $\bar{\Lambda}(I)$ denote the part of $\Lambda(I)$ where $|F(I, \eta)| > c_2^{-1}$. If (I_r, η_r) corresponds to a point of $\bar{\Lambda}(I_r)$, then, according to the KAM theory, there is an invariant curve at a distance larger than c_3^{-1} from the point $\tilde{\xi} = 0$, $\eta = \eta_r$. We call the domain surrounded by this curve a stability island of the Poincaré map. The area of this island is larger than c_4^{-1}. Returning from $\tilde{\xi}$, η to the original variables I, η, we find that the area of the stability island is estimated from below as $c_4^{-1}\varepsilon$.

The boundary of the stability island (an invariant curve) is a section of the invariant torus on the energy level of the original system. The volume of the domain surrounded by this torus is larger than $C_1^{-1}\varepsilon$. The variation of $\hat{I}$ inside this domain is smaller than $C_2\varepsilon$.

9 Example: stable periodic trajectories and stability islands in the problem of the motion of charged particles in the parabolic model of magnetic field

9.1 The model

The parabolic model (see, e.g. [10]) is one of the simplest models of the magnetic field in the Earth magnetotail. Introduce a right Cartesian coordinate system $Ox\xi q$ with the origin located in the Earth's equatorial plane, the Earth being located between the origin and the Sun; the Ox-axis lies in the equatorial plane and is directed towards the Earth, and the Oq-axis is orthogonal to the equatorial plane. In this coordinate system the magnetic field vector has the form $\mathbf{B} = (B_0 q/L, 0, B_n)$. Here B_0, B_n, L are positive constants. The field lines of this field are parabolas $B_n x - B_0 q^2/(2L) = \text{const}$ (see Figure 3).

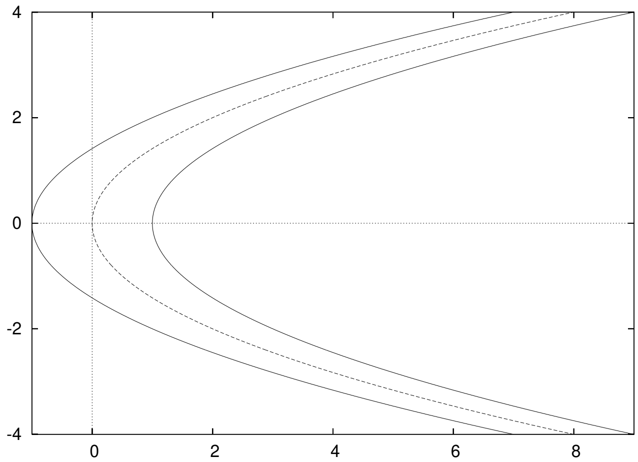

Figure 3: Field lines of the magnetic field in the parabolic model.

The vector potential of the magnetic field has the form $\mathbf{A} = (0, B_n x - B_0 q^2/(2L), 0)$. The motion of a charged particle in such a field is described by a Hamiltonian system with the following Hamiltonian function:

$$H = \frac{1}{2m}\left[y^2 + \left(\eta - \frac{e}{c}\left(B_n x - B_0 \frac{q^2}{2L}\right)\right)^2 + p^2\right]. \tag{53}$$

Here m and e are the mass and the charge of the particle, c is the speed of light. The pairs of canonically conjugated variables are (y, x), (η, ξ), (p, q). The Hamiltonian does not depend on ξ, and hence $\eta \equiv \text{const}$ along the motion. Without restricting the generality we put $\eta \equiv 0$.

Introduce new pairs of canonically conjugated coordinates $(y_1, \varepsilon^{-1} x_1), (p_1, q_1)$, new time t_1 and a new Hamiltonian H_1 according to the formulas:

$$
\begin{aligned}
x_1 &= \varepsilon\frac{x}{\sqrt{\rho L}}, & y_1 &= \frac{y}{mv},\\
q_1 &= \frac{q}{\sqrt{\rho L}}, & p_1 &= \frac{p}{mv},\\
t_1 &= t\frac{v}{\sqrt{\rho L}}, & H_1 &= \frac{H}{mv^2}.
\end{aligned}
$$

Here v is a typical velocity of the particle, $\rho = cmv/(eB_0)$ is a typical Larmor radius, $\varepsilon = \frac{B_n}{B_0}\sqrt{L/\rho}$; $v, \rho = \text{const}$. In the new variables the Hamiltonian takes the form (we omit the subscript "1"):

$$
H = \frac{1}{2}\left[y^2 + p^2 + \left(x - \frac{1}{2}q^2\right)^2\right]. \tag{54}
$$

Following [10], we consider the case $\varepsilon \ll 1$ (it is valid for ions). In this case, p, q are the fast variables, and y, x are the slow on1es. The phase portrait of the fast system is represented in Figures 4a and 4b for $x > 0$ and $x < 0$ respectively.

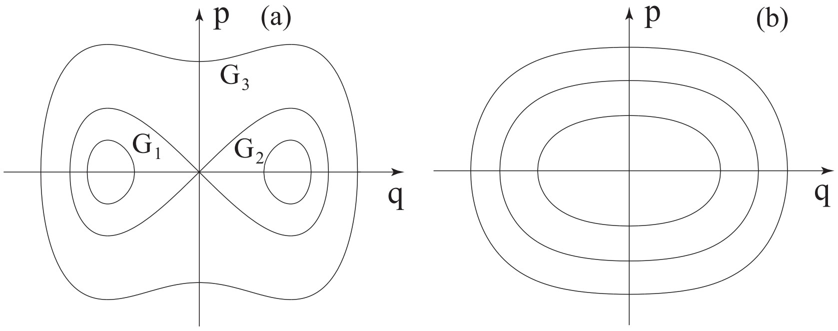

Figure 4: Typical phase portraits of the fast system for a) $x > 0$ and b) $x < 0$.

Consider the motion on the energy level $H = 1/2$. On the configuration plane (x, q) the motion is possible between two parabolas (see Figure 3). The two field lines are also the zero velocity curves (zvc). On the plane of the slow variables the motion is possible in the domain obtained by the union of the half-disk $\{x, y : x^2 + y^2 \leq 1,\ x \leq 0\}$ and the half-strip $\{x, y : |y| \leq 1,\ x > 0\}$. The uncertainty curve Γ is the semicircle $\{x, y : x^2 + y^2 = 1, x \geq 0\}$. The phase trajectories on the fast plane that lie inside the domains G_1 and G_2 correspond to the points of the plane of the slow variables with $x^2 + y^2 > 1$ (see Figure 4a). The phase trajectories that lie in the domain G_3 correspond to the points on the plane of the slow variables with $x^2 + y^2 < 1$, $x > 0$.

The phase portrait of the slow system at $H = 1/2$ is presented in Figure 5 (see [10]). The boundary of the domain of possible motion on the portrait corresponds to the motion with zero value of the "action". For points of the plane of the slow variables with $y = \pm 1$, $x > 0$, the corresponding phase point on the fast plane in the adiabatic approximation always coincides with one of the two stable fixed points of the fast system. For points of the semicircle $\{x, y : x^2 + y^2 = 1,\ x < 0\}$, the corresponding phase point on the fast plane is always in the only stable fixed point of the fast system. The stable fixed point on the phase portrait of the slow system has the coordinates $y = 0$, $x = x_e \approx 0.65$.

In [10], the chaotic dynamics in the domain filled with trajectories of the slow system that cross the uncertainty curve was found and studied.

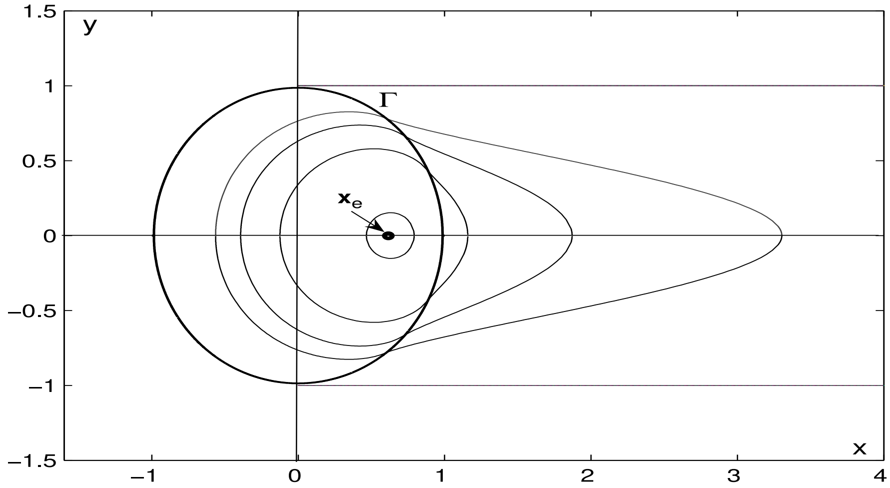

Figure 5: Phase plane of the slow variables.

9.2 Formulas for the dynamics in the slow system and separatrix crossings

The following formulas are valid for the values S, Θ_*, a_*, α introduced in Sections 2, 5, and 6 [10]:

$$S = \frac{8}{3}x^{3/2}, \qquad \Theta_* = 4y_* x_*^{1/2}, \tag{55}$$

$$a_* = x_*^{-1/2}, \qquad \alpha = \tfrac{2}{\pi}y_*. \tag{56}$$

The modified "action" $\hat{I}$ in the domain G_i is [10]

$$\hat{I} = \frac{4}{3\pi}(2\mathcal{E})^{1/4} f_i(k), \tag{57}$$

where

$$f_3(k) = (1-k^2)\mathbf{K}(k) + (2k^2-1)\mathbf{E}(k),$$
$$f_{1,2}(k) = 2(1-k^2)k\mathbf{K}(1/k) + (2k^2-1)k\mathbf{E}(1/k),$$
$$k = \sqrt{\frac{1}{2}\left(1 + \frac{x}{\sqrt{2\mathcal{E}}}\right)}, \quad \mathcal{E} = \frac{1}{2}\left(p^2 + (x - q^2/2)^2\right);$$

$\mathbf{K}(\,\cdot\,), \mathbf{E}(\,\cdot\,)$ are the complete elliptic integrals of first and second kinds, respectively.

It turns out that in the considered specific problem we have: $\gamma_1 < 0, \gamma_2 > 0, |\gamma_1| \gg 1, \gamma_2 \ll 1$ (for the definition of γ_i, see (25)). Therefore, according to Section 7.2, there are no non-symmetric stable periodic trajectories. Symmetric stable periodic trajectories correspond to the two intervals (41) of the variable η. The corresponding intervals of the variable $u = \alpha\pi\cot\pi\eta$ are of equal small length $2/|\gamma_1|$ (see (40)). Hence, the number of stable periodic trajectories is much smaller than the number of unstable periodic trajectories. Now, the left endpoint of the second one of these two intervals is the point of the minimum of the function f in (44). Therefore, the variation of f on this interval is much smaller than its variation on the first interval. Hence, the second interval corresponds to a much smaller number of stable periodic trajectories than the first one. Taking into account the relations between γ_1 and γ_2, we find for K_{sm} (see (45)) in the main approximation:

$$K_{sm} = \frac{1}{2}\int_{\Xi_0} \frac{4}{\alpha\pi^2}\,\mathrm{d}\hat{I}. \tag{58}$$

The quantities $\hat{I}$ and x_* are related as $2\pi\hat{I} = S(x_*)$. Using (55), (56), we obtain

$$\hat{I} = \frac{1}{2\pi}\,\frac{8}{3}x_*^{3/2} = \frac{4}{3\pi}(1-y_*^2)^{3/4}.$$

Hence,

$$K_{sm} = \int_{\Xi_0} \frac{\mathrm{d}\hat{I}}{\pi y_*} = \frac{2}{\pi^2}\int_{\Xi_0} (1-y_*^2)^{-1/4}\,\mathrm{d}y_*. \tag{59}$$

Let $v = y_*^2$. Then

$$K_{sm} = \frac{1}{\pi^2}\int_{v_1}^{v_2} (1-v)^{-1/4}v^{-1/2}\mathrm{d}v, \tag{60}$$

where v_1 and v_2 are the values of $v = y_*^2$ at the endpoints of Ξ_0. In particular, if we take for Ξ_0 the complete interval of values of $\hat{I}$ corresponding to the separatrix crossings, we have $v_1 = 0$, $v_2 = 1$. Accordingly, for the value K_c of the function K_{sm} we find:

$$K_c = \frac{1}{\pi^2}\int_0^1 (1-v)^{-1/4}v^{-1/2}\mathrm{d}v = \frac{1}{\pi^2}\mathrm{B}(1/2,3/4) = \frac{1}{\pi^2}\,\frac{\Gamma(1/2)\Gamma(3/4)}{\Gamma(5/4)}. \tag{61}$$

Here, as usual, $\mathrm{B}(\,\cdot\,)$ and $\Gamma(\,\cdot\,)$ denote the beta and gamma functions respectively. Using the reflection formula for the gamma function [15], we find

$$K_c = \frac{1}{\pi^2}\sqrt{\pi}\frac{1}{\Gamma(5/4)\Gamma(1/4)}\,\frac{\pi}{\sin(\pi/4)} = \sqrt{\frac{2}{\pi}}\,\frac{1}{4(\Gamma(5/4))^2} \approx 0.21\,. \tag{62}$$

In the next section we consider solutions with initial conditions $p = y = 0, q = q_0$. On the energy level $H = 1/2$, for the corresponding initial value x_0 of x we have the relation $1/2(x_0 - q_0^2/2)^2 = 1/2$ and, hence $x_0 = q_0^2/2 \pm 1$. Take the "minus" sign in the latter expression. Calculate for such a solution the value $v = y_*^2$ in the adiabatic approximation. We have

$$v = y_*^2 = 1 - x_*^2 = 1 - \left(\frac{3\pi}{4}\,\hat{I}\right)^{4/3},$$

$$\mathcal{E} = H - \frac{1}{2}y^2 = \frac{1}{2}, \quad k = \sqrt{\frac{1}{2}\left(1 + \frac{x_0}{\sqrt{2\mathcal{E}}}\right)} = \frac{|q_0|}{2},$$

$$\hat{I} = \frac{4}{3\pi}(2\mathcal{E})^{1/4}f_3(k) = \frac{4}{3\pi}f_3(|q_0|/2).$$

Hence,

$$v = 1 - (f_3(|q_0|/2))^{4/3}. \tag{63}$$

9.3 Results of the numeric studies

For the exact system the 2D surface $y = 0$ will be used as a surface of the Poincaré section, despite it is not globally transversal to the phase flow. Figure 6 displays a representation of a part of this surface. The horizontal variables are q and p and x is the vertical one. We see that, beyond the fact that it is not a global Poincaré section, to every point (q, p) on the strip $|p| < 1$ correspond two possible values of x.

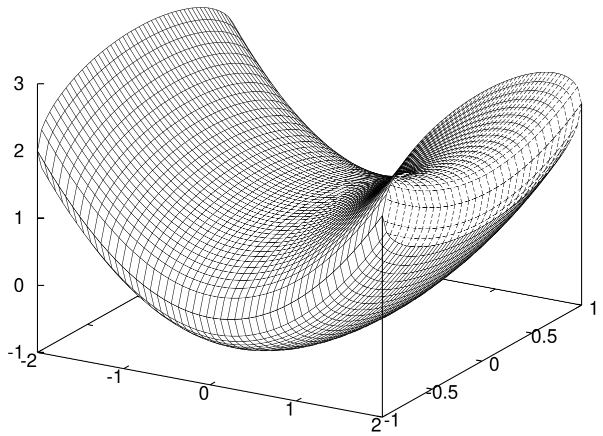

Figure 6: The surface $y = 0$ used as the surface of the Poincaré section.

These effects are illustrated in Figure 7 for $\varepsilon = 0.04$. The same value of ε has been used up to Figure 13. For smaller ε many pictures look quite wild. The initial point $\varepsilon^{-1}x = 10, q = 0, y = 0, p > 0$ seems to be on an invariant torus. The section by the surface $y = 0$, disregarding the value of x and the sign of $\dot{y}$ is shown to the left. The second plot contains only the points for which $\dot{y} > 0$. Third one contains points with $\dot{y}$ either positive or negative, but only for the values of $x < x_e$ (see Section 9.1). The rightmost plot displays only points with $\dot{y} > 0$ and $x < x_e$.

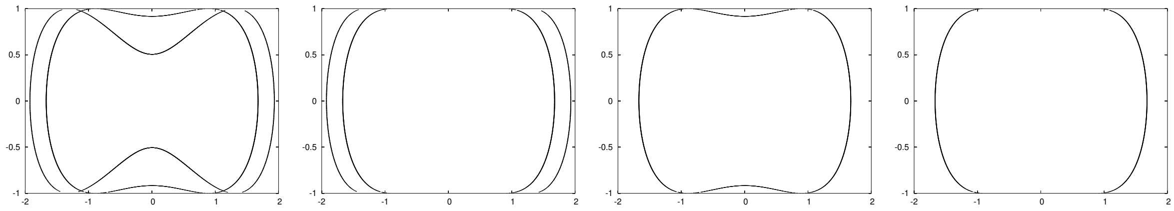

Figure 7: Various versions of the Poincaré section. See the text.

Using a 3D representation, Figure 8 shows a Poincaré section, disregarding the value of x and the sign of $\dot{y}$ at $y = 0$. It has been obtained using initial conditions of the form $q = y = 0$ and $\varepsilon^{-1}x = 3, 4, \ldots, 15$ and computing 10^4 iterates and then points with the same initial conditions for q and y but with $\varepsilon^{-1}x < 3$ and step 0.05. We note that most of these points are in chaotic regions and their orbits approach large values of $\varepsilon^{-1}x$. Typically, the computation is stopped when $\varepsilon^{-1}x > 10^4$ (or when the number of integration steps using a Taylor method at order 28 exceeds 10^6 steps to compute a Poincaré iterate) to obtain this figure. In the figure there are regions where the density of points is smaller. They correspond to a neighborhood of the lines where $y = 0$ is no longer transversal to the flow.

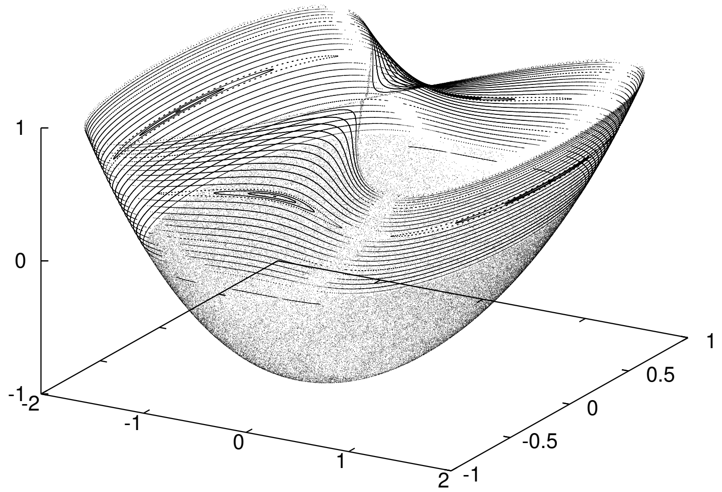

Figure 8: The Poincaré section of phase trajectories with initial conditions $q = y = 0$, $\varepsilon^{-1}x = 3, 4, \ldots, 15$, and $\varepsilon^{-1}x < 3$ with step 0.05. The axes are the same as in Figure 6.

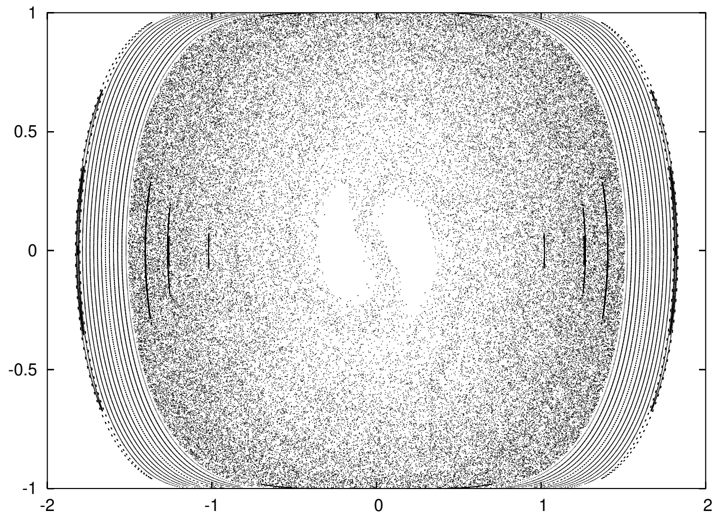

Figure 9: The Poincaré section of Figure 8 projected onto the (q, p)-plane.

Close to $x = x_e, y = 0$ the system has a periodic orbit. It oscillates mildly around the plane $y = 0$ and intersects it four times. This can be clearly seen in Figure 8, with the corresponding narrow island around it, in the zone of regular motion. Other tiny islands appear inside the chaotic region and the study of them is the main goal of this paper. Some of them can be also seen in Figure 8. However, for a better understanding, we shall consider only the (q, p) projections of the Poincaré section, using the constrains $x < x_e, \dot{y} > 0$. This can be seen in Figure 9. The outer part of Figure 9 corresponds to trajectories without separatrix crossings. This part is mainly filled with segments of invariant curves as it should be by the Arnold perpetual adiabatic invariance theorem (see, e.g. [13]). The inner part of Figure 9 is a chaotic sea [10].

The two central holes inside the chaotic region correspond to points coming from large values of $\varepsilon^{-1}x$ (either in $q > 0$ or in $q < 0$). The objects inside the chaotic sea which look as segments of fat curves are actually islands with a fixed elliptic point at its center.

A part of Figure 9 is shown in Figure 10, left. Four islands are clearly seen in that plot. A magnification of the rightmost one is shown in Figure 10, right. Because the island is narrow and close to a parabola with horizontal axis, instead of (q, p) we display $(q + 0.395p^2, p)$.

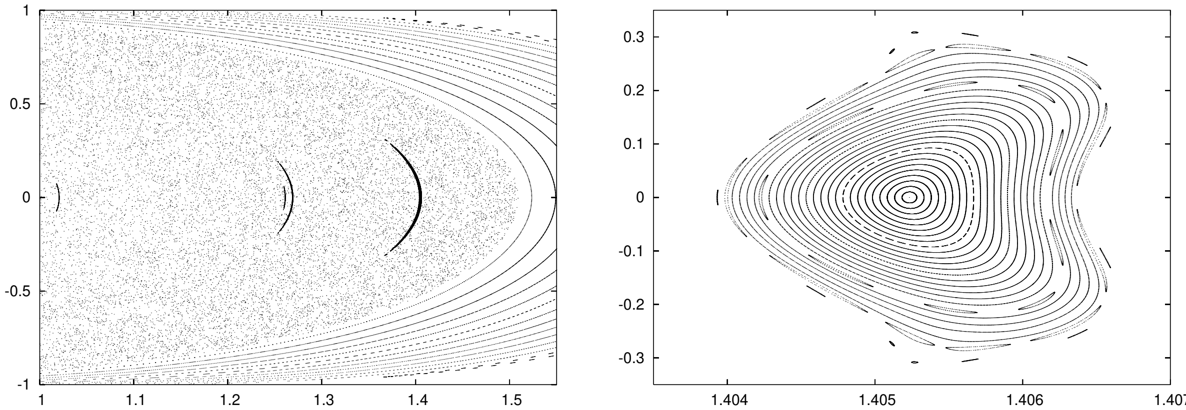

Figure 10: A zoom of the previous picture (left) and magnification of the rightmost island (right).

For a clear identification of the different zones in the configuration plane $(\varepsilon^{-1}x, q)$ we show, in Figure 11, the results presented in Figure 9 in these new variables. The continuous line corresponds to the left boundary of the zero velocity curve (zvc) $p = y = 0$, while the discontinuous line shows the location of $\dot{y} = 0$. One can check once more the sharp transition between regular and chaotic motion. The islands seen in this picture are hardly visible in Figure 9: they are on the top close to $p = 1$. Note that there are islands of period 2, without points on $q = 0$. The two zones without points of the chaotic sea which appear close to $\varepsilon^{-1}x = -25$ correspond to the two holes near the center of Figure 9. They will be filled only if orbits reaching extremely large values of $\varepsilon^{-1}x$ (and, hence, extremely large values of the return time) are computed.

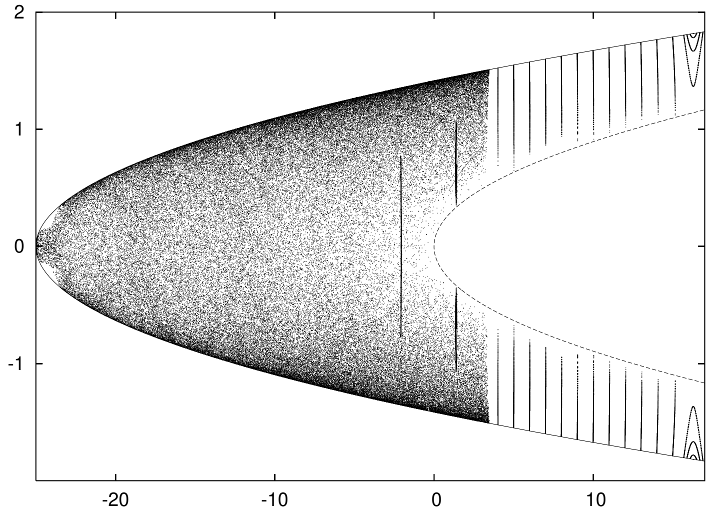

Figure 11: Results of Figure 9 projected onto the configuration plane $(\varepsilon^{-1}x, q)$.

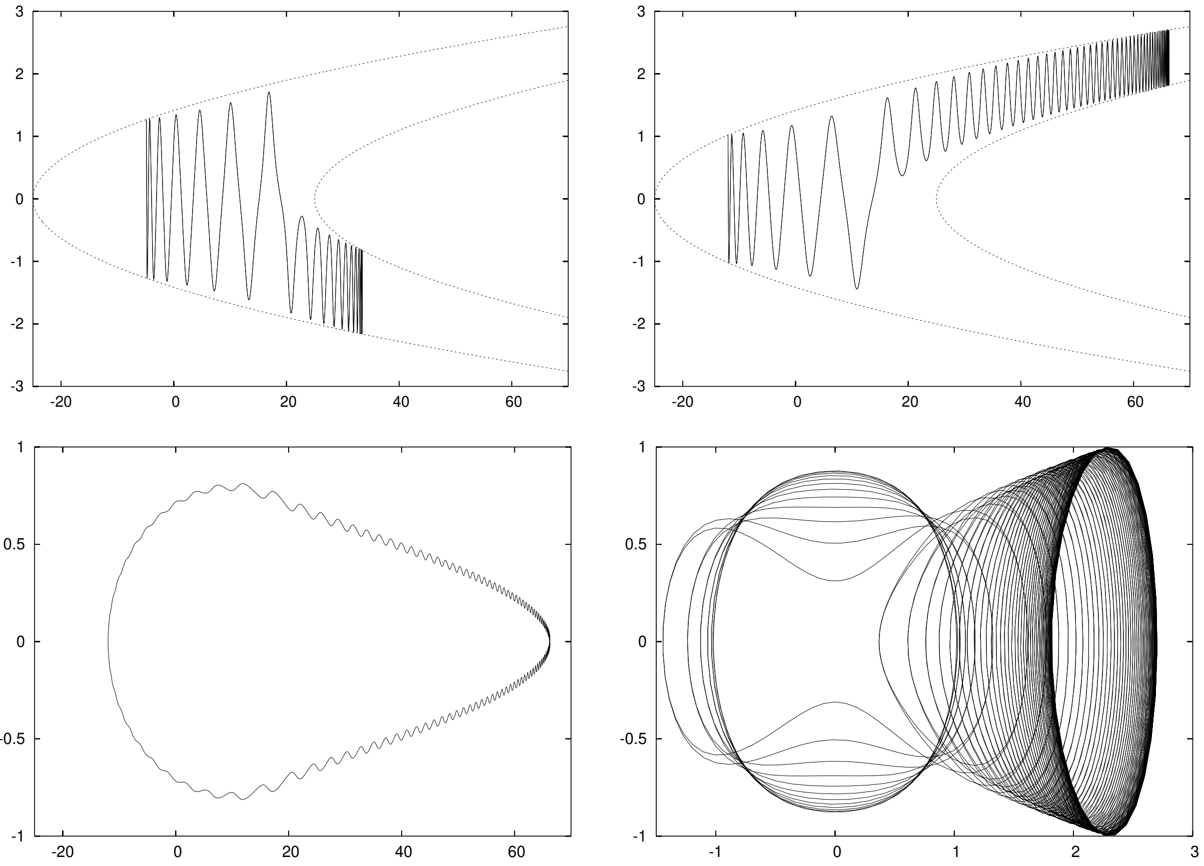

Figure 12: Various projections of stable periodic orbits. See the text.

As an illustration, Figure 12, top left, shows the first (going from left to right) stable periodic orbit of Figure 10 left, and on the right part the third one. On the bottom we display, for the first of these orbits, the projections on $(\varepsilon^{-1}x, y)$ (left) and on (q, p) (right). On the $(\varepsilon^{-1}x, y)$ plane, it can be seen that the orbit is close to the one theoretically predicted (except for some minor oscillations). On the (q, p) plane the transition of the fast system across the separatrix is clearly seen.

We have computed simple periodic orbits (i.e., fixed points of the Poincaré map) with initial conditions on the zvc: $y = p = 0$. They appear on Figures 9 and 10 on the horizontal axis. Due to the symmetry it is enough to start with $q > 0$. We note that for $y = q = p = 0$ there is a periodic orbit fully contained in the (x, y) plane.

In a similar way one can compute periodic orbits starting on the $q = 0$ axis. Again, due to the symmetry, it is enough to use $p > 0$. To grasp the wild character of the flow Figure 13 shows, on the left, the first image under the Poincaré map of the line $q = 0$ with values of $p \in (-1, 1)$ and step size 10^{-5}. On the right we display, in $\log_{10}$ scale, the maximum value of $\varepsilon^{-1}|x|$ reached (lower curve) and the return time (upper curve) as a function of p. The plot would be similar taking points of the zvc ($p = 0$ in this section).

To compute p.o. on the zvc we have restricted our interest to the domain $q \in [1, \sqrt{2}]$. (Smaller values of q correspond to extremely large return times.) This is enough to illustrate the theory. This range of q is scanned using a control on the distance between consecutive points, in order to follow carefully all the foldings of the image. Steps in q as small as 10^{-12} are accepted. The results of the computation are shown in Table 1. As

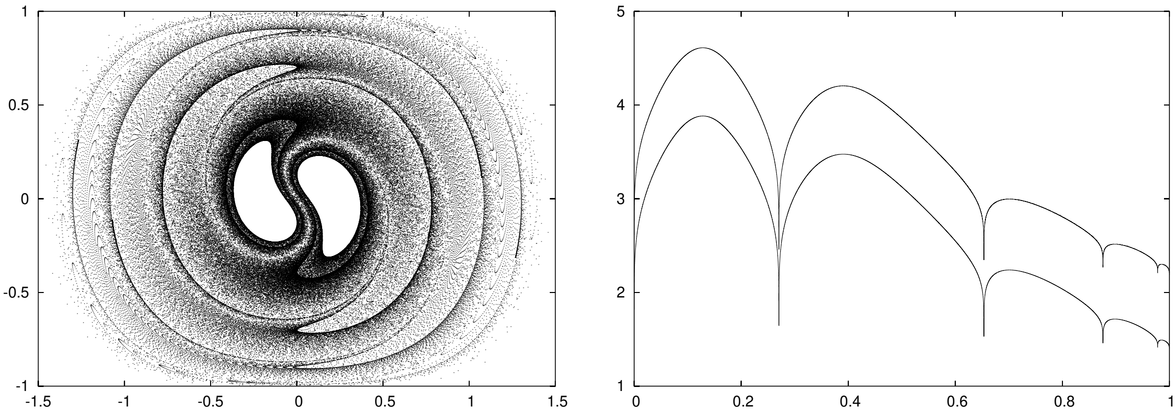

Figure 13: The first image under the Poincaré map of the line $q = 0$ with values of $p \in (-1, 1)$ and step size 10^{-5} (left). The maximum value of $\varepsilon^{-1}|x|$ reached (lower curve) and the return time (upper curve) as a function of p (right). In the vertical axes the $\log_{10}$ scale has been used.

predicted by the theory, both the total number of p.o. and the number of stable ones (s.p.o.) behave as ε^{-1}.

ε	periodic orbits	stable periodic orbits	K_{sm}/ε
0.00025	24235	370	396
0.001	6351	94	99
0.0025	2662	38	39.6
0.01	632	11	9.9
0.04	144	4	2.5

Table 1: Number of periodic orbits.

The p.o. in $p = 0$ appear also (if we display the period or the maximal value of x along the orbit) in bumps similar to the ones displayed in Figure 13, right. Decreasing ε the number of bumps increases like ε^{-1}. On each bump the behavior of the system is similar.

A representation of the location of the p.o. is displayed on Figure 14, left. On it the cumulative number of p.o. which are found from $q = 1$ on, multiplied by the corresponding value of ε, is displayed as a function of q. The curves are shown for $\varepsilon = 0.01, 0.0025, 0.001$ and 0.00025. The smaller is the value of ε, the smaller is the effect of the bumps. Then, on the right part of Figure 14 we have collected the distribution of p.o. inside a bump as follows. If ε is small the bumps are also small. The extrema of the bump can be taken as the places where the return time has a local minima (or, equivalently, the maximal x is minimum or, also, the trace of the nearby p.o. is also a minimum). If q_1 and q_2 are the extrema of some bump ($q_1 < q_2$), and q^* denotes the position of a p.o., it can be referred to the bump by means of the parameter $\tilde{q} = (q^* - q_1)/(q_2 - q_1)$. Collecting all the values of $\tilde{q}$ for the different p.o. we can get the desired distribution. This is plotted to the right in Figure 14. Despite a total of 359 complete bumps is found for $q \in [1, \sqrt{2}]$ for $\varepsilon = 0.00025$ (this reduces to 89 for $\varepsilon = 0.001$), only the bumps for $q \in [1, 1.1]$ have been used. The reason is that for that range of q the computed value of $\tilde{q}$ is close enough to the theoretical

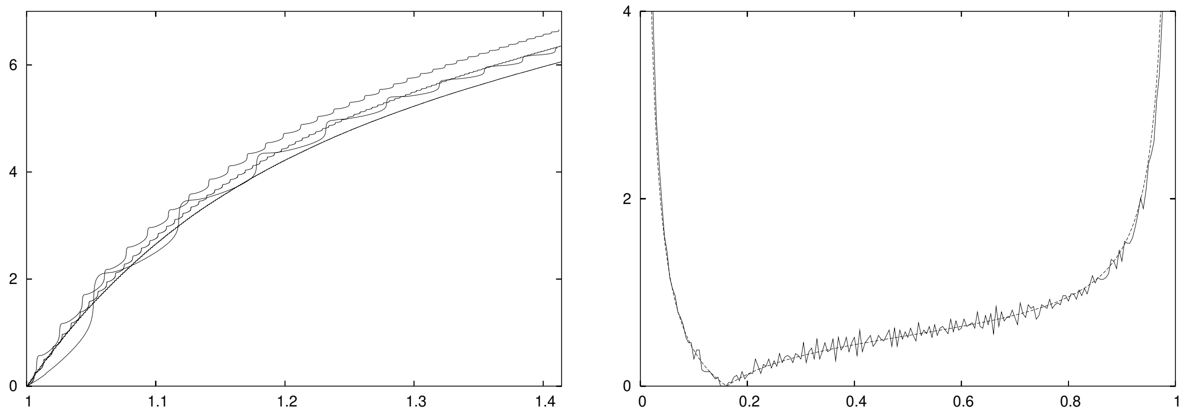

Figure 14: Left: the cumulative number of p.o. found from $q = 1$ on, multiplied by the corresponding value of ε as a function of q. Right: the distribution of p.o. inside one bump and the theoretical curve.

parameter η introduced in Section 5. In this range there are 58 full bumps which contain 10373 p.o. We selected 200 intervals of equal length in the $\tilde{q}$ variable. The scale has been normalized to have total area equal to 1. In the same plot, and in discontinuous lines, the theoretical density of the p.o. as a function of η is also shown. It is given by an expression of the form (47)

$$\rho(\eta) = C\,|c - 1/\tan(\pi\eta)|\,,$$

where $c = 2(\gamma_1 + \gamma_2)/(\pi\gamma_1\gamma_2)$ (in notations of Section 7) and C is a normalization constant. The approximate values $c = 1.8, C = 0.3$ have been used. Due to the relatively small number of p.o. the experimental density shows some irregularities, but the global agreement is remarkable. We recall that close to the endpoints of the interval the theoretical approximation fails. The density becomes zero at $\frac{1}{\pi}\tan^{-1}(1/c) \approx 0.16$, in good agreement with numerical results.

Concerning the s.p.o., in each bump one should find two narrow intervals in η (41) which can contain such orbits. The largest one is close to $\eta = 1/2$. However, as the intervals are narrow and the transformation from $\tilde{q}$ to η depends also on the location of the bump, it is not suitable to look at results considering all the bumps together. As before, it is enough to use only a part of the bumps (for instance, with $q_0 \in [1, 1.1]$). It is checked that the stable p.o. are located in the interval $\tilde{q} \in [0.5, 0.515]$. A very narrow interval of s.p.o. appears also near $\tilde{q} = 0.2$, but it contains less than 2% of the total number of s.p.o. This is in agreement with the theoretical prediction in Section 9.2.

We compare the total number of s.p.o. to the theoretical predictions as follows. Orbits starting on the zvc for $q_0 \in [1, \sqrt{2}]$ cross the separatrix ($x^2+y^2 = 1$) at values of $y \in [y_1, y_2]$. Let $v_i = y_i^2$. According to (63), we have in the adiabatic approximation

$$v_1 = 1 - (f_3(1/\sqrt{2}))^{4/3} = 1 - \left(\frac{1}{2}\mathbf{K}(1/\sqrt{2})\right)^{4/3} \approx 0.096\,,$$

$$v_2 = 1 - (f_3(1/2))^{4/3} = 1 - \left(\frac{3}{4}\mathbf{K}(1/2) - \frac{1}{2}\mathbf{E}(1/2)\right)^{4/3} \approx 0.570\,.$$

Calculating the integral in (60) with these values of $v_{1,2}$ we obtain $K_{sm} \approx 0.099$. The quantity K_{sm}/ε is, in the main approximation, the number of s.p.o. of the family **F1** (or

F2) that start from zvc with $q_0 \in [1, \sqrt{2}]$ and $q_0 \in [-\sqrt{2}, -1]$. It is also equal in the main approximation to the number of s.p.o. of the two families that start from the zvc with $q_0 \in [1, \sqrt{2}]$. For K_{sm}/ε we find the values, which are in good agreement with the numerical results (see Table 1).

Acknowledgements

The authors are grateful to L.M.Zelenyi for useful discussions. The work was supported in part by grants RFBR 06-01-00117, 05-01-01119, and NSh-1312.2006.1. C.S. has been supported by grants BFM2003-09504-C02-01, MTM2006-05849/Consolider (Spain) and CIRIT 2005 SGR-1028 (Catalonia).

Appendix. The planar periodic orbit

Here we discuss the special role played by the periodic orbit sitting on $(q,p) = (0,0)$. As it is contained in the (x,y) plane, we shall call it the *planar* p.o. If $y(0) = 0$, it is given by $x = \cos(\varepsilon t)$, and the normal variational equation is given (as a second order equation) by $\ddot{\xi} = \cos(\varepsilon t)\xi$. This is a particular case of Mathieu equation, with zero average. Let $M = \int_0^\pi \sqrt{\sin(\tau)}d\tau \approx 2.39628$. For small ε the monodromy matrix can be approximately written as the product of rotation by the angle M/ε and an hyperbolic matrix of dominant eigenvalue $\exp(M/\varepsilon)$. Figure 15, left, displays the variation of the trace tr of the monodromy matrix as a function of $1/\varepsilon$. In the horizontal axis we display $1/\varepsilon$, while in the vertical one $\sinh^{-1}(tr)$ is shown. It is straightforward to show that, despite infinitely many intervals of stability occur they are extremely narrow. More precisely: stability domains appear near values of $1/\varepsilon$ of the form $M^{-1}(k+1/2)\pi, k \in \mathbb{Z}, k > 0$, while the width of these intervals is, up to a constant factor, of the form $\exp(-M/\varepsilon)$.

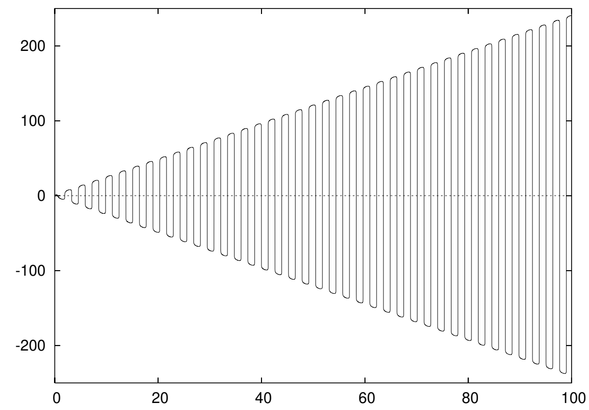

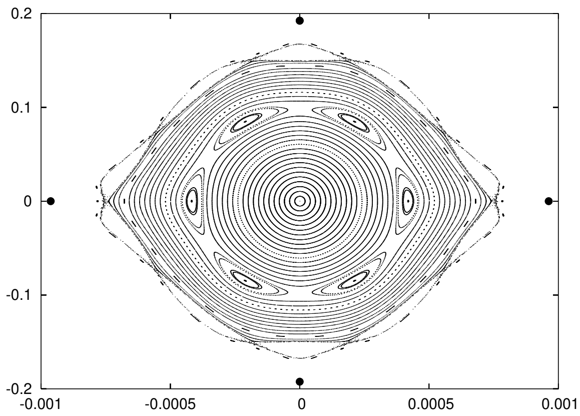

Figure 15: Left: variation of the trace of the monodromy matrix as a function of $1/\varepsilon$. Right: a stability island.

In each one of these stability intervals there is an invariant island around $(0,0)$ in the (q,p) plane. As an example, Figure 15 right shows the island for $\varepsilon = 0.5155$, in the stability domain with the left endpoint at $\varepsilon = 0.5136759883096067$ and the width 2.25×10^{-3}. Even for that large value of ε the width of the island in q is small (less than

0.002). Furthermore there exists a period 4 p.o. (displayed as black big points) which is hyperbolic. The presence of nearby hyperbolic periodic orbits has been checked for other values of ε in the stability domains. Hence, when the planar p.o. becomes stable (for these narrow intervals) there appear other unstable p.o. which play a similar role. Using an index argument in a suitable ball containing the island inside, one can prove that the global dynamics outside this ball is only affected for very narrow intervals of initial conditions. From now on we shall not consider these stability intervals.

Dependence of the return time on the initial value of q contains certain characteristic structures that we call bumps, see Figure 13, right. Figure 16 shows, in the upper part, a sample of results, and several details in the lower part. Concretely, on the left upper plot we present the results for trajectories with initial conditions at $p = 0$ and $q \in [0, \sqrt{2}]$ for $\varepsilon = 0.3, 0.2, 0.1, 0.04$. We plot the logarithm of the return time as a function of the initial value of q. The smaller ε is, the higher are the bumps and the smaller is the distance between endpoints of a bump, as it was said before. For instance, for $\varepsilon = 0.04$ the maximal return time from the zvc exceeds 10^7. In the central upper plot we show, for $q \in [1, \sqrt{2}]$ the logarithms of the return time multiplied by ε for $\varepsilon = 0.04, 0.01, 0.0025$. The curves on these plots tend to a limit curve when $\varepsilon \to 0$. On the right upper part we show the end of the big bump close to $q = 1.15$ for $\varepsilon = 0.04$, displaying the return time as a function of q on the narrow window $[1.15027, 1.1502744]$. Five ends of small bumps can be seen to the left of the endpoint of the big bump, one of them very close to this endpoint. All this detailed structure is not visible in the previous plot (the middle upper one).

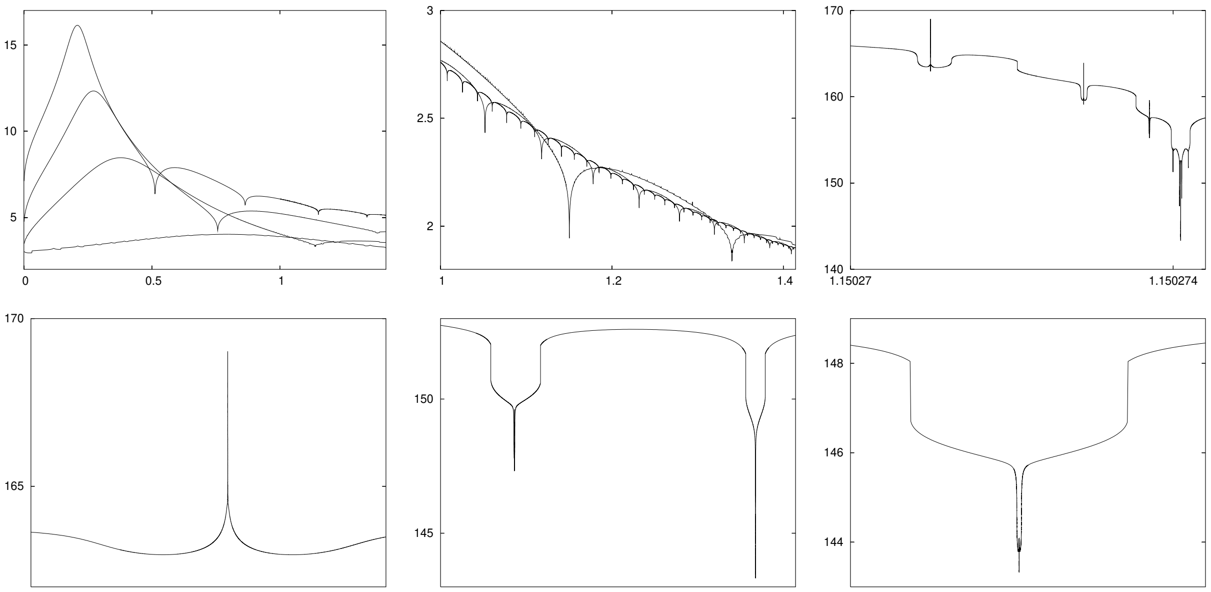

Figure 16: The bumps and their structure. See the text for a detailed explanation.

In the lower part of the figure, and from left to right we show a detail of the end of the leftmost small bump of the previous plot (window $[1.150270992 \pm 2 \times 10^{-9}]$), a view of the end of the rightmost small bump together with the end of the big bump (window $[1.150274085 \pm 5 \times 10^{-9}]$) and a great enlargement of the end of the big bump (window $[1.150274092745 \pm 25 \times 10^{-12}]$. The vertical jumps in the return time, clearly visible in last plot, are due to the fact that $p_x = 0$ is not everywhere transversal to the flow, as it was discussed (see Figure 7 right, for instance). To the right of the endpoint of the big bump the pattern of small bumps is almost symmetric to the one displayed here.

Now we pass to the reasons for the creation of big and small bumps in geometric terms. Taking, for instance, an initial point on the zvc, it can approach the separatrix $x^2 + y^2 = 1$ moving close to the planar p.o. Then it can move back to smaller values of x, or it can enter one of the *branches* of the region $x > 1$, either the upper one or the lower one. A critical orbit would tend to the planar one along its stable manifold. Hence, looking at the maximal value of x along the orbit, it would never exceed 1. Furthermore, moving on the stable manifold of the planar p.o. it would reach a point with $y = 0, \dot{y} > 0$ close to $x = -1$.

Hence, the endpoints of the big bumps can be seen as the place where there is a minimum of the maximum value of x along the orbit (as a function of the initial value of q in the zvc) or as the place where orbits switch from entering the upper branch to the lower one or vice versa (see below for an additional explanation). Or, in other words, to switching between entering one or the other of the lobes at the crossing of the separatrix.

Small bumps are related to the crossing of the separatrix when we go outside, to the circulation region, that is, x decreases and enters the domain $x < 1$. An orbit entering from one of the branches to the region $x < 1$ can also approach the planar p.o. along the stable manifold. This occurs depending on the phase it has when it reaches the maximal value of x in one of the branches. As it changes quickly for ε small, there are many small bumps inside one big bump. Again, entering $x < 1$ we can pass close to the planar p.o. and leave its vicinity following one of the two branches of their unstable manifold.

References

[1] Neishtadt A I , Sidorenko V V and Treschev D V 1997 Stable periodic motions in the problem of passage through a separatrix *Chaos* **7** 2-11

[2] Neishtadt A I , Sidorenko V V and Treschev D V 2001 On stability islands in the domain of separatrix crossings *Nonlinear Mechanics* ed V M Matrosov, V V Rumyantsev *et al* (Moscow: Fizmatlit) pp 192-203 (in Russian)

[3] Neishtadt A I, Simó C, Treschev D V, and Vasiliev A A 2006 Stability islands in domains of separatrix crossings in slow-fast Hamiltonian systems *Proceedings of the V.A. Steklov Mathematical Institute*, to be submitted.

[4] Timofeev A V 1978 On the constancy of an adiabatic invariant when the nature of the motion changes *Sov. Phys. JETP* **48** 656-659

[5] Cary J R , Escande D F and Tennyson J 1986 Adiabatic invariant change due to separatrix crossing *Phys. Rev.* **A34** 4256-4275

[6] Neishtadt A I 1986 Change of an adiabatic invariant at a separatrix *Sov.J.Plasma Phys.* **12** 568-573

[7] Cary J R , Skodje R T 1989 Phase change between separatrix crossings *Physica D* **36** 287-316

[8] Neishtadt A I 1987 On the change in the adiabatic invariant on crossing a separatrix in systems with two degrees of freedom *PMM USSR* **51** 586-592

[9] Neishtadt A I and Vasiliev A A 2005 Phase change between separatrix crossings in slow-fast Hamiltonian systems *Nonlinearity* **18** 1393-1406

[10] Büchner J , Zelenyi L M 1989 Regular and chaotic charged particle motion in magnetotail like field reversals, 1, Basic theory of trapped motion *Journal of Geophysical Research* **94**(A9) 11821-11842

[11] Wisdom J 1985 A perturbative treatment of motion near the 3/1 commensurability *Icarus* **63**(2) 272-289

[12] Neishtadt A I and Sidorenko V V 2004 Wisdom system: dynamics in the adiabatic approximation, *Celestial Mechanics and Dynamical Astronomy* **90** 307-330

[13] Arnold V I , Kozlov V V and Neishtadt A I 1988 *Mathematical aspects of classical and celestial mechanics (Encyclopedia of mathematical sciences 3)* (Berlin: Springer)

[14] Tal F A , Vanden-Eijnden E 2006 Transition state theory and dynamical corrections in ergodic systems *Nonlinearity* **19** 501-509

[15] Abramowitz M , Stegun I A 1965 *Handbook of Mathematical Functions, With Formulas, Graphs, and Mathematical Tables* (Dover Publications)